Band structure of semimagnetic $Hg_{1-y}Mn_yTe$ quantum wells

E. G. Novik,[1,*] A. Pfeuffer-Jeschke,[1] T. Jungwirth,[2,†] V. Latussek,[1] C. R. Becker,[1] G. Landwehr,[1] H. Buhmann,[1] and L. W. Molenkamp[1]

[1]*Physikalisches Institut der Universität Würzburg, Am Hubland, 97074 Würzburg, Germany*

[2]*Institute of Physics ASCR, Cukrovarnická 10, 162 53 Praha 6, Czech Republic*

(Received 14 September 2004; revised manuscript received 25 March 2005; published 12 July 2005)

The band structure of semimagnetic $Hg_{1-y}Mn_yTe/Hg_{1-x}Cd_xTe$ type-III quantum wells (QW's) has been calculated using an eight-band $\boldsymbol{k}\cdot\boldsymbol{p}$ model in an envelope function approach. Details of the band structure calculations are given for the Mn-free case ($y=0$). A mean-field approach is used to take the influence of the *sp-d* exchange interaction on the band structure of QW's with low Mn concentrations into account. The calculated Landau level fan diagram and the density of states of a $Hg_{0.98}Mn_{0.02}Te/Hg_{0.3}Cd_{0.7}Te$ QW are in good agreement with recent experimental transport observations. The model can be used to interpret the mutual influence of the two-dimensional confinement and the *sp-d* exchange interaction on the transport properties of $Hg_{1-y}Mn_yTe/Hg_{1-x}Cd_xTe$ QW's.

DOI: 10.1103/PhysRevB.72.035321 PACS number(s): 73.21.Fg, 71.20.Nr, 71.70.Ej, 71.70.Gm

I. INTRODUCTION

Recently, numerous spin-related observations have been published which involve optical and transport experiments on diluted magnetic, semiconducting heterostructures and quantum wells (QW's).[1–5] The correct interpretation of these effects requires a detailed knowledge of the underlying band structure. This is especially important for narrow-gap semiconductors,[6] because strong band mixing prevents a simple interpretation of optical and transport results by means of a parabolic band model which might be still applicable for most wide-gap materials such as GaAs or InGaAs.[7,8]

Here, we concentrate on the band structure calculations of $HgTe/Hg_{1-x}Cd_xTe$ quantum wells. This material has some interesting properties: depending on the QW width (d_W), the QW has either a *normal* or *inverted* band structure when $d_W<6$ nm or $d_W>6$ nm, respectively. In the latter case the conduction band exhibits Γ_8 symmetry which leads to a strong Rashba spin-orbit splitting in QW's with an asymmetrical confinement potential.[6,9] Additionally, the spin splitting of the subbands can be enhanced by introducing magnetic ions (Mn) in the QW structure—e.g., $Hg_{1-y}Mn_yTe/Hg_{1-x}Cd_xTe$. It should be noted that in II-VI semiconductors, Mn is incorporated into the crystal lattice isoelectrically and does not act as a donor or an acceptor. Therefore, Mn ions act primarily as a magnetic but not as a Coulomb impurity and mobilities achieved for these QW structures with low Mn concentrations are comparable with those for nonmagnetic structures.

This paper is organized as follows: In Sec. II a detailed description of the model used for the band structure calculations is presented. In Sec. II A, we consider the model for nonmagnetic as well as for magnetic QW's at zero external magnetic field. This model is used to calculate the subband energy dispersion of $Hg_{0.98}Mn_{0.02}Te/Hg_{0.3}Cd_{0.7}Te$ and $HgTe/Hg_{0.3}Cd_{0.7}Te$ QW's. In Sec. II B, the band structure model for a $HgTe/Hg_{1-x}Cd_xTe$ QW in an external magnetic field is described. This model is extended in Sec. II C in order to take the influence of the *sp-d* exchange interaction on the band structure of magnetic QW's into account. The Landau level fan diagram and the density of states of $Hg_{0.98}Mn_{0.02}Te/Hg_{0.3}Cd_{0.7}Te$ QW are compared with recent transport experiments, and Sec. III summarizes the results. Details of the boundary conditions, calculations for different growth directions and strain as well as piezoelectric effects are discussed in the Appendixes A, B and C, respectively.

II. BAND STRUCTURE MODEL

A. $B=0$

The band structure model we use is based on an envelope-function approach introduced by Burt.[10] The total wave function is expanded in terms of band-edge ($\boldsymbol{k}=0$) Bloch functions u_n:

$$\Psi(\boldsymbol{r}) = \sum_n F_n(\boldsymbol{r}) u_n(\boldsymbol{r}), \tag{1}$$

where $F_n(\boldsymbol{r})$ are the envelope functions. u_n is assumed to be the same in the barrier and well layers. Assuming translation invariance in the plane perpendicular to the growth direction (z axis) F_n can be represented as

$$F_n = \exp[i(k_x x + k_y y)] f_n(z), \tag{2}$$

where k_x and k_y are the wave vector components in the plane of the QW. The envelope functions and the energy levels near $\boldsymbol{k}=0$ are determined within the framework of $\boldsymbol{k}\cdot\boldsymbol{p}$ theory by solving a system of coupled differential equations:[11,12]

$$\sum_{n'} (H_{nn'} + V(z)\delta_{nn'}) f_{n'}(z) = \sum_{n'} \left(\sum_{\alpha,\beta}^{x,y,z} k_\alpha D_{nn'}^{\alpha\beta} k_\beta + \sum_{\alpha}^{x,y,z} P_{nn'}^{\alpha} k_\alpha + E_{n'}(z)\delta_{nn'} + V(z)\delta_{nn'} \right) f_{n'}(z) = E \cdot f_n(z), \tag{3}$$

where n and n' are the summation indices for the sum over

the dimensionality of the chosen basis set, $E_{n'}(z)$ are the respective band-edge potentials, and $V(z)$ is the self-consistently calculated Hartree potential. The momentum matrix elements $P^{\alpha}_{nn'}$ describe the coupling between the n and n' bands exactly, while the $D^{\alpha\beta}_{nn'}$ elements consider their coupling to the remote bands in second-order perturbation theory.[13,14]

In order to solve the system of differential equations in Eq. (3) the functions $f_n(z)$ are expanded in terms of the complete basis set $\{g_i(z)\}$:

$$f_n(z) = \sum_i c^i_n g_i(z), \quad i = 0,1,2, \ldots, \tag{4}$$

where $g_i(z)$ are derived from Legendre polynomials and the maximum value of i defines the accuracy of the solution of the eigenvalue problem.[6] Polynomials up to 15th order are sufficient to describe the problem to the desired accuracy. The expansion in Eq. (4) leads to a matrix representation of the eigenvalue problem where the eigenvectors with components c^i_n and the corresponding eigenvalues are obtained by matrix diagonalization (see Appendix A for more details).

In narrow-gap HgTe based structures, the strong coupling between the lowest conduction and the highest valence bands causes mixing of the electronic states and induces nonparabolicity in the conduction bands. These effects were taken into account exactly by Kane[12] in the framework of the $\boldsymbol{k}\cdot\boldsymbol{p}$ theory. In order to consider the coupling between the Γ_6, Γ_7, and Γ_8 bands we choose the usual eight-band basis set (see Refs. 11 and 15)

$$\begin{aligned}
u_1(\boldsymbol{r}) &= |\Gamma_6, +1/2\rangle = S\uparrow,\\
u_2(\boldsymbol{r}) &= |\Gamma_6, -1/2\rangle = S\downarrow,\\
u_3(\boldsymbol{r}) &= |\Gamma_8, +3/2\rangle = (1/\sqrt{2})(X+iY)\uparrow,\\
u_4(\boldsymbol{r}) &= |\Gamma_8, +1/2\rangle = (1/\sqrt{6})[(X+iY)\downarrow - 2Z\uparrow],\\
u_5(\boldsymbol{r}) &= |\Gamma_8, -1/2\rangle = -(1/\sqrt{6})[(X-iY)\uparrow + 2Z\downarrow],\\
u_6(\boldsymbol{r}) &= |\Gamma_8, -3/2\rangle = -(1/\sqrt{2})(X-iY)\downarrow,\\
u_7(\boldsymbol{r}) &= |\Gamma_7, +1/2\rangle = (1/\sqrt{3})[(X+iY)\downarrow + Z\uparrow],\\
u_8(\boldsymbol{r}) &= |\Gamma_7, -1/2\rangle = (1/\sqrt{3})[(X-iY)\uparrow - Z\downarrow].
\end{aligned} \tag{5}$$

The total angular momentum is then given by $j=1/2$ or $j=3/2$.

For the chosen basis set, the Hamiltonian $H_{nn'}$ in Eq. (3) for a two-dimensional system with [001] growth direction takes the following form:[6]

$$H = \begin{pmatrix}
T & 0 & -\frac{1}{\sqrt{2}}Pk_+ & \sqrt{\frac{2}{3}}Pk_z & \frac{1}{\sqrt{6}}Pk_- & 0 & -\frac{1}{\sqrt{3}}Pk_z & -\frac{1}{\sqrt{3}}Pk_-\\
0 & T & 0 & -\frac{1}{\sqrt{6}}Pk_+ & \sqrt{\frac{2}{3}}Pk_z & \frac{1}{\sqrt{2}}Pk_- & -\frac{1}{\sqrt{3}}Pk_+ & \frac{1}{\sqrt{3}}Pk_z\\
-\frac{1}{\sqrt{2}}k_-P & 0 & U+V & -\bar{S}_- & R & 0 & \frac{1}{\sqrt{2}}\bar{S}_- & -\sqrt{2}R\\
\sqrt{\frac{2}{3}}k_zP & -\frac{1}{\sqrt{6}}k_-P & -\bar{S}^{\dagger}_- & U-V & C & R & \sqrt{2}V & -\sqrt{\frac{3}{2}}\tilde{S}_-\\
\frac{1}{\sqrt{6}}k_+P & \sqrt{\frac{2}{3}}k_zP & R^{\dagger} & C^{\dagger} & U-V & \bar{S}^{\dagger}_+ & -\sqrt{\frac{3}{2}}\tilde{S}_+ & -\sqrt{2}V\\
0 & \frac{1}{\sqrt{2}}k_+P & 0 & R^{\dagger} & \bar{S}_+ & U+V & \sqrt{2}R^{\dagger} & \frac{1}{\sqrt{2}}\bar{S}_+\\
-\frac{1}{\sqrt{3}}k_zP & -\frac{1}{\sqrt{3}}k_-P & \frac{1}{\sqrt{2}}\bar{S}^{\dagger}_- & \sqrt{2}V & -\sqrt{\frac{3}{2}}\tilde{S}^{\dagger}_+ & \sqrt{2}R & U-\Delta & C\\
-\frac{1}{\sqrt{3}}k_+P & \frac{1}{\sqrt{3}}k_zP & -\sqrt{2}R^{\dagger} & -\sqrt{\frac{3}{2}}\tilde{S}^{\dagger}_- & -\sqrt{2}V & \frac{1}{\sqrt{2}}\bar{S}^{\dagger}_+ & C^{\dagger} & U-\Delta
\end{pmatrix}, \tag{6}$$

where

$$k^2_{\parallel} = k^2_x + k^2_y, \quad k_{\pm} = k_x \pm ik_y, \quad k_z = -i\partial/\partial z,$$

$$T = E_c(z) + \frac{\hbar^2}{2m_0}[(2F+1)k^2_{\parallel} + k_z(2F+1)k_z],$$

TABLE I. Band structure parameters of HgTe and CdTe at $T=0$ K (Ref. 6 and 9).

	E_g	Δ	$E_P=2m_0P^2/\hbar^2$	F	γ_1	γ_2	γ_3	κ
HgTe	−0.303 eV	1.08 eV	18.8 eV	0	4.1	0.5	1.3	−0.4
CdTe	1.606 eV	0.91 eV	18.8 eV	−0.09	1.47	−0.28	0.03	−1.31

$$U = E_v(z) - \frac{\hbar^2}{2m_0}(\gamma_1 k_\parallel^2 + k_z\gamma_1 k_z),$$

$$V = -\frac{\hbar^2}{2m_0}(\gamma_2 k_\parallel^2 - 2k_z\gamma_2 k_z),$$

$$R = -\frac{\hbar^2}{2m_0}(\sqrt{3}\mu k_+^2 - \sqrt{3}\bar{\gamma}k_-^2),$$

$$\bar{S}_\pm = -\frac{\hbar^2}{2m_0}\sqrt{3}k_\pm(\{\gamma_3,k_z\} + [\kappa,k_z]),$$

$$\tilde{S}_\pm = -\frac{\hbar^2}{2m_0}\sqrt{3}k_\pm\left(\{\gamma_3,k_z\} - \frac{1}{3}[\kappa,k_z]\right),$$

$$C = \frac{\hbar^2}{m_0}k_-[\kappa,k_z]. \quad (7)$$

$[A,B]=AB-BA$ is the usual commutator and $\{A,B\}=AB+BA$ is the anticommutator for the operators A and B; P is the Kane momentum matrix element; $E_c(z)$ and $E_v(z)$ are the conduction and valence band edges, respectively; Δ is the spin-orbit splitting energy; and γ_1, γ_2, γ_3, κ, and F describe the coupling to the remote bands and result in the μ and $\bar{\gamma}$ parameters according to $\mu=(\gamma_3-\gamma_2)/2$ and $\bar{\gamma}=(\gamma_3+\gamma_2)/2$. Only the terms with nonspherical (cubic) symmetry in the Hamiltonian are proportional to the warping parameter μ. The case of $\mu=0$ corresponds to the axial approximation. The intrinsic inversion asymmetry is neglected in the Hamiltonian because this effect is very small in HgTe-based structures.[16] The band structure parameters for HgTe and CdTe at $T=0$ K are listed in Table I. The dependence of the band gap (E_g) of $Hg_{1-x}Cd_xTe$ on the temperature and composition x is determined from the empirical expression according to Laurenti *et al.*[17] The valence band offset between HgTe and CdTe is taken to be equal to 570 meV at $T=0$ K, in agreement with recent experiments,[18] and is assumed to vary linearly with x.[19]

We assume that the band structure parameters change abruptly (step like) at the interfaces. The problem for such structures with abrupt interfaces was solved by Burt[10] with an exact envelope-function approach. Accordingly, the correct operator ordering in the Hamiltonian provides an unambiguous determination of the interface boundary conditions. Previously, this approach was used successfully by Foreman.[20] He demonstrated that the boundary conditions obtained from an *ad hoc* symmetrization of the Hamiltonian give nonphysical solutions for the heavy-hole bands, while Burt's approach leads to correct physical results. This was also confirmed by Meney *et al.*[21] for the valence band structure of InGaAsSb/AlGaSb QW when the lowest conduction band is included in the Hamiltonian explicitly or treated as a remote band. The matrix elements of the Hamiltonian in Eq. (6), which describe the Γ_8 and Γ_7 states and their couplings, are similar to those derived by Foreman. With the assumption that the Kane momentum matrix element P is constant throughout the structure, Foreman's[20,22] boundary conditions at the interfaces can easily be extended to the eight-band case (see Appendix A for more details).[21] It should be noted that the Hamiltonian in Eq. (6) contains additional off-diagonal elements proportional to $[\kappa(z),k_z]$, which are equal to zero in the bulk structures.

So far, we have only considered the case of $HgTe/Hg_{1-x}Cd_xTe$ QW's with (001) orientation. However, HgTe based structures have also been investigated with orientations other than (001)—for example, (112) heterostructures.[18,23] The electronic properties of such systems depend strongly on the growth direction. An extension of the model to QW's of a given (kkl) orientation can be obtained using the approach of Los *et al.*:[24] the set of basis functions [Eqs. (5)] is changed to a set which adopts the symmetry of the problem, and thus the transformed Hamiltonian once again has the form of Eq. (6), while the matrix elements [Eqs. (7)] contain additional terms depending on the structure orientation.[6] The exact formulas for these terms are given in Appendix B. Also strain and piezoelectric effects can be included, as discussed in Appendix C.

During the last two decades much attention has been paid to the theoretical and experimental understanding of diluted magnetic semiconductors (DMS's), both in bulk[25–27] as well as in low-dimensional structures.[27] Extensively studied examples of this category are $A^{II}_{1-y}Mn_yB^{VI}$ alloys, in which the group-II component is replaced randomly by the transition metal Mn.[28] So far, most research on magnetic two-dimensional structures has been done on wide-gap DMS materials.[2,4] Previous work on magnetic two-dimensional electron gas (2DEG) in narrow-gap II-VI DMS's can be found in Refs. 29 and 30. In the present work we consider QW's with magnetic ions (Mn) in narrow-gap $Hg_{1-y}Mn_yTe/Hg_{1-x}Cd_xTe$ QW's. The two-dimensional confinement in the DMS-based layer combined with the exchange interaction between localized Mn magnetic moments and mobile band electrons makes such structures quite interesting candidates for the study of their electronic and magnetic properties.

The band structure of $Hg_{1-y}Mn_yTe/Hg_{1-x}Cd_xTe$ QW's in the absence of a magnetic field can be calculated similarly as that of nonmagnetic QW's; cf. the description above. The only difference is that the band structure parameters for the well now depend on the Mn concentration.[28]

In Fig. 1 the zero-field subband dispersion $E(k_\parallel)$ of n-type $Hg_{0.98}Mn_{0.02}Te/Hg_{0.3}Cd_{0.7}Te$ (a), (b), (d) and HgTe/

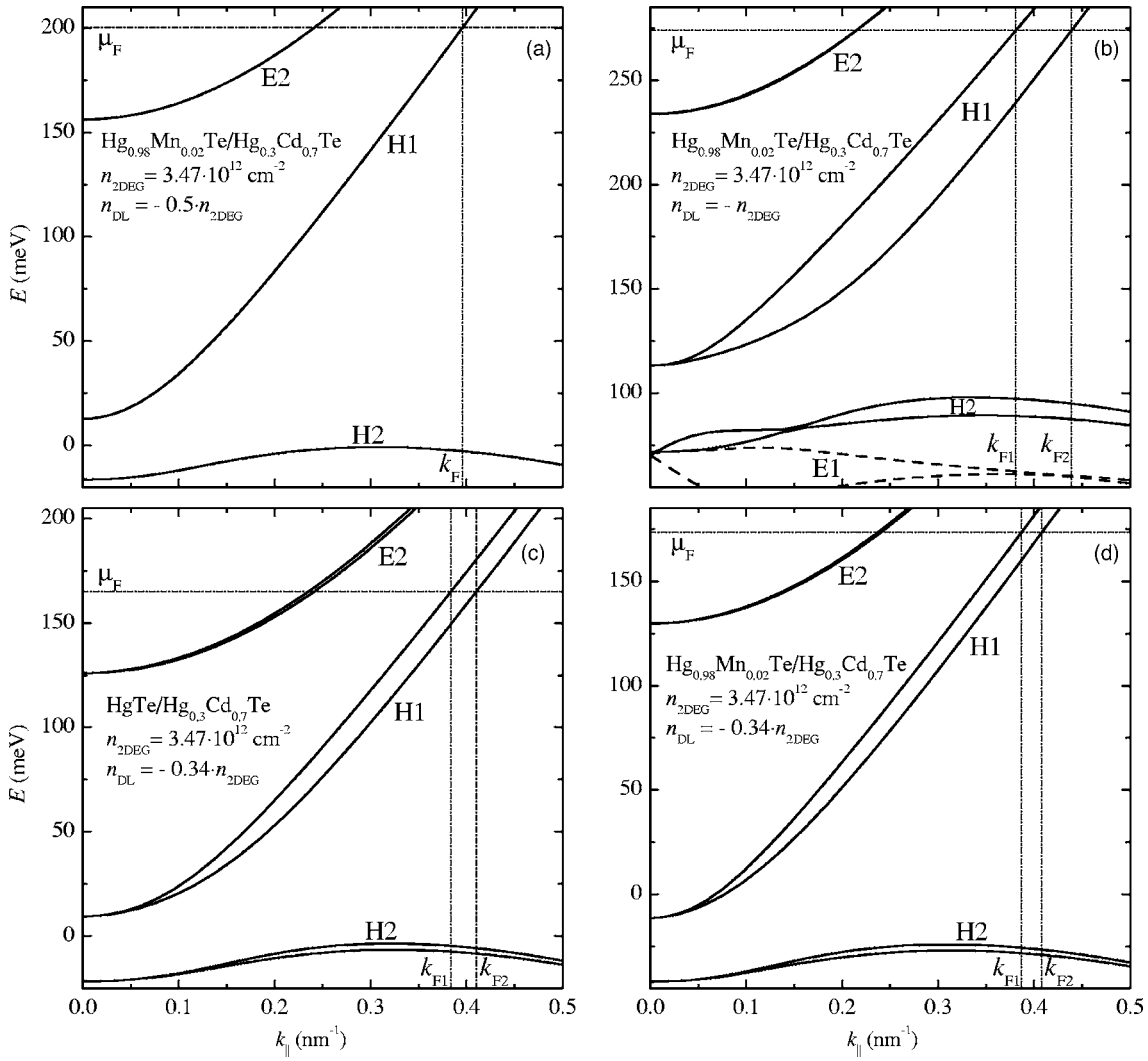

FIG. 1. Band structure of *n*-type (a) symmetrical and (b), (d) asymmetrical $Hg_{0.98}Mn_{0.02}Te/Hg_{0.3}Cd_{0.7}Te$ QW's, as well as (c) an asymmetrical $HgTe/Hg_{0.3}Cd_{0.7}Te$ QW, all with d_W=12.2 nm at T=4.2 K. $k_{F1}=k_F(H1-)$ and $k_{F2}=k_F(H1+)$. Here the $k_\|$ vector is $k_\|(1,0)$; however, the difference between $E(k_\|(1,0))$ and $E(k_\|(1,1))$ is less then 6 meV at k_F and the k dependence shows qualitatively the same behavior. The $E1$ subband [which corresponds to an interface bound state in the quantum well (Ref. 31)] is shown as dashed lines.

$Hg_{0.3}Cd_{0.7}Te$ (c) (001) QW's are presented. The temperature T and the QW's width d_W are set at 4.2 K and 12.2 nm, respectively. Figure 1(a) corresponds to a $Hg_{0.98}Mn_{0.02}Te/Hg_{0.3}Cd_{0.7}Te$ QW with symmetrically *n*-type modulation-doped barriers, while only the barrier on the substrate side is doped for the case presented in Fig. 1(b). In the calculations it is assumed that (i) all donors in the doped layer are ionized, (ii) the charge density is constant in this region, and (iii) all electrons are transferred to the QW. The depletion charge in the doped layers is taken to be $n_{DL}=-n_{2DEG}$ for an asymmetrically and $n_{DL}=-0.5n_{2DEG}$ for a symmetrically doped structure, respectively.[6] (n_{2DEG} denotes the charge density of the 2DEG in the QW and is chosen to be $n_{2DEG}=3.47\times10^{12}$ cm^{-2} for the calculations presented here.) The eigenvalue [Eq. (3)] and Poisson equations for the two-dimensional charge carriers in the QW are solved self-consistently for both cases. The depletion charge in the doped layers, which is assumed to be fixed at the levels indicated above, is included into the boundary conditions to solve the Poisson equation.[32] Then the Hartree potential is determined according to the charge distribution of electrons in the QW, which is given by the summation over all conduction band states i and all components n of the envelope functions $f_n(z)$:

$$\rho^e(z) = -e\sum_i^{\mathrm{CB}} \frac{1}{(2\pi)^2} \int \sum_{n=1}^{8} |f_n^i(z)|^2 f_{\mathrm{F}}(E_i) d^2k, \qquad (8)$$

where e is the electron charge and $f_{\mathrm{F}}(E)$ is the Fermi function. Here, we assume that $n_{2DEG}<0$ and $n_{DL}>0$. In analogy, we have, for the holes,

$$\rho^{\mathrm{p}}(z) = +e\sum_i^{\mathrm{VB}} \frac{1}{(2\pi)^2} \int \sum_{n=1}^{8} |f_n^i(z)|^2 [1-f_{\mathrm{F}}(E_i)] d^2k. \qquad (9)$$

In this case the summation index i runs over all valence band states and $n_{DL}<0$. The self-consistent Hartree potential for

zero magnetic field is then used to calculate the Landau levels of the 2DEG (see description below).

From Figs. 1(a) and 1(b) one observes that both QW's exhibit an inverted band structure. The conduction band includes two occupied subbands (labeled as $H1$ and $E2$); the lower conduction subband ($H1$) exhibits a heavy-hole character at $k_\parallel=0$. The electronlike $E1$ subband lies, in this case, below the $H2$ subband and is now one of the valence subbands. The $H1$ and $H2$ subbands are not split for the symmetric QW [case (a)]; however, for the asymmetric QW, a spin-orbit splitting (in the following denoted as a spin splitting as is common in the literature) of the $H2$ subband as well as a pronounced splitting of the $H1$ subband are visible. The splitting of $H1$ is 33.4 meV at k_{F1} and 30.9 meV at k_{F2}, respectively. The carrier concentrations in the $H1-$ and $H1+$ subbands for the asymmetric QW, after self-consistency has been obtained, are 1.18×10^{12} and 1.55×10^{12} cm^{-2}, respectively. This large spin-orbit splitting, usually called Rashba splitting, of the $H1$ state in an asymmetric QW was demonstrated to be an unique feature of type-III QW's in the inverted band regime.[9] Experimentally values up to 30 meV have indeed been observed.[33]

The subband dispersions $E(k_\parallel)$ of $HgTe/Hg_{0.3}Cd_{0.7}Te$ and $Hg_{0.98}Mn_{0.02}Te/Hg_{0.3}Cd_{0.7}Te$ QW's are shown in Figs. 1(c) and 1(d), where n_{DL} is taken to be equal to $-0.34n_{2DEG}$; i.e., 66% of the electron density in the QW stems from the top and 34% from the bottom doped layer. The band structures of the nonmagnetic (c) and magnetic (d) QW's differ notably in the subband separation at $k_\parallel=0$; the separation between the $E2$ and $H1$ subbands is about 24 meV smaller for nonmagnetic QW. The Rashba splitting of the $H1$ subband is 15.5 meV for the nonmagnetic and 13.1 meV for the magnetic QW's for $k_\parallel(1,0)$. The corresponding values are 14.2 meV and 12.2 meV for $k_\parallel(1,1)$. This relatively small difference arises because the actual band gap (Δ_{H1-H2}) changes only by 2% upon introduction of Mn.

B. $B\neq0$

In an external magnetic field perpendicular to the plane of the 2DEG, the electronic bands are split into a series of Landau levels. The effects of a magnetic field $\boldsymbol{B}=(0,0,B)$ can be incorporated by a Peierls substitution[14,34] in the Hamiltonian [Eq. (6)] as follows:

$$\boldsymbol{k}\rightarrow\boldsymbol{k}'=-i\nabla+\frac{e}{\hbar}\boldsymbol{A}, \tag{10}$$

where $\boldsymbol{A}$ is the magnetic vector potential, $\boldsymbol{B}=\nabla\times\boldsymbol{A}$. One possible Landau gauge for $\boldsymbol{B}\parallel z$ is $\boldsymbol{A}=(0,Bx,0)$. The operator $\boldsymbol{k}'$ satisfies the following gauge-invariant relation:

$$\boldsymbol{k}'\times\boldsymbol{k}'=-i\frac{e}{\hbar}\boldsymbol{B}. \tag{11}$$

From now on, we drop the prime for simplicity. Subsequently, k_x and k_y are rewritten such that[14,16]

$$a=\frac{l_c}{\sqrt{2}}k_-,\quad a^\dagger=\frac{l_c}{\sqrt{2}}k_+, \tag{12}$$

where $l_c=\sqrt{\hbar/eB}$ is the magnetic length and a and $a^\dagger$ are, respectively, the annihilation and creation operators for the harmonic oscillator functions φ_n, where[16]

$$a\varphi_n=\sqrt{n}\varphi_{n-1},\quad a^\dagger\varphi_n=\sqrt{n+1}\varphi_{n+1},\quad a^\dagger a\varphi_n=n\varphi_n. \tag{13}$$

Here, $n=0,1,2,\ldots$ are the eigenvalues of the operator $a^\dagger a$. Thus, we can present the Hamiltonian in Eq. (6) as a function of a, $a^\dagger$, $k_z=-i\partial/\partial z$, the band structure parameters, and their z dependence.

Additionally, the Zeeman term H^Z has to be included in the Hamiltonian [Eq. (6)]. As shown by Weiler,[16] this leads to the following matrix:

$$H^Z=\hbar\frac{eB}{m_0}\begin{pmatrix}
\frac{1}{2} & 0 & 0 & 0 & 0 & 0 & 0 & 0\\
0 & -\frac{1}{2} & 0 & 0 & 0 & 0 & 0 & 0\\
0 & 0 & -\frac{3}{2}\kappa & 0 & 0 & 0 & 0 & 0\\
0 & 0 & 0 & -\frac{1}{2}\kappa & 0 & 0 & -\frac{\kappa+1}{\sqrt{2}} & 0\\
0 & 0 & 0 & 0 & \frac{1}{2}\kappa & 0 & 0 & -\frac{\kappa+1}{\sqrt{2}}\\
0 & 0 & 0 & 0 & 0 & \frac{3}{2}\kappa & 0 & 0\\
0 & 0 & 0 & -\frac{\kappa+1}{\sqrt{2}} & 0 & 0 & -(\kappa+\frac{1}{2}) & 0\\
0 & 0 & 0 & 0 & -\frac{\kappa+1}{\sqrt{2}} & 0 & 0 & (\kappa+\frac{1}{2})
\end{pmatrix}. \tag{14}$$

In the axial approximation we now assume that the total wave function can be written as[6]

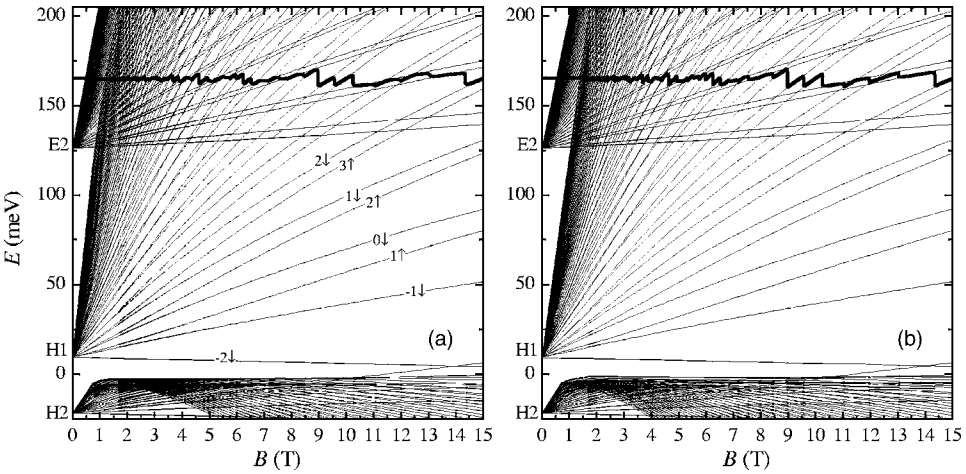

FIG. 2. Landau levels of the $E2$, $H1$, and $H2$ subbands for an n-type $HgTe/Hg_{0.3}Cd_{0.7}Te(001)$ QW as a function of magnetic field (a) with and (b) without the axial approximation. $d_W=12.2$ nm, $n_{2DEG}=3.47\times10^{12}$ cm^{-2}, $n_{DL}=-0.34n_{2DEG}$, and $T=4.2$ K. The thick line represents the chemical potential. The Landau levels are labeled with quantum numbers N, and the arrows ($\uparrow$,$\downarrow$) indicate the dominant spin orientation of the state.

$$\Psi_N(\boldsymbol{r}) = \exp\left(-i\frac{X}{l_c^2}y\right)\begin{pmatrix} f_1(z) & \varphi_{n_1} \\ f_2(z) & \varphi_{n_2} \\ f_3(z) & \varphi_{n_3} \\ f_4(z) & \varphi_{n_4} \\ f_5(z) & \varphi_{n_5} \\ f_6(z) & \varphi_{n_6} \\ f_7(z) & \varphi_{n_7} \\ f_8(z) & \varphi_{n_8} \end{pmatrix} = \exp\left(-i\frac{X}{l_c^2}y\right)\begin{pmatrix} f_1^{(N)}(z) & \varphi_N \\ f_2^{(N)}(z) & \varphi_{N+1} \\ f_3^{(N)}(z) & \varphi_{N-1} \\ f_4^{(N)}(z) & \varphi_N \\ f_5^{(N)}(z) & \varphi_{N+1} \\ f_6^{(N)}(z) & \varphi_{N+2} \\ f_7^{(N)}(z) & \varphi_N \\ f_8^{(N)}(z) & \varphi_{N+1} \end{pmatrix}, \tag{15}$$

where $X=-l_c^2k_y$ is the center-of-motion coordinate and restrictions on the quantum numbers N on the right-hand side can be derived straightforwardly from Eqs. (13). Since $n=0,1,2,\ldots$, the new quantum number $N=-2,-1,0,\ldots$. For all quantum numbers N a system of (up to eight) coupled differential equations has to be solved. For $N=-2$ the system is reduced to one equation that corresponds to a state with pure heavy-hole character. Nonaxially symmetric systems can be treated by taking the coupling between the solutions of the axially symmetric problem [Eq. (15)] into account.[35] The form of the coupling depends on the symmetry along the growth direction and can be included by the substitution of a linear combination of the Ψ_N wave functions:[6]

$$\Psi_K(\boldsymbol{r}) = \sum_N c_N\Psi_N(\boldsymbol{r}), \tag{16}$$

with $K=-2,-1,0,1$ and $N=K,K+4,K+8,\ldots$ for a (001)-oriented structure (C_4 symmetry); $K=-2,-1,0$ and $N=K,K+3,K+6,\ldots$ for a (111) structure (C_3 symmetry); $K=-2,-1$ and $N=K,K+2,K+4,\ldots$ for a (110) structure (C_2 symmetry); and $K=-2$ and $N=K,K+1,K+2,\ldots$ for other growth directions. A system of coupled differential equations for the envelope functions $f_j^{(N)}$ has to be solved for each value of the quantum number K. The Hamiltonian matrix elements $\langle\varphi_{n_i}|H_{ij}|\varphi_{n_j}\rangle$ are determined using Eqs. (12) and (13). For the numerical solution of the problem, an expansion of the envelope functions $f_j^{(N)}$ is used in analogy with the case without a magnetic field [Eq. (4)].

The Landau level spectra of a $HgTe/Hg_{0.3}Cd_{0.7}Te(001)$ QW calculated with and without the axial approximation are shown in Figs. 2(a) and 2(b), respectively, for the structure whose corresponding subband dispersion is presented in Fig. 1(c). Since the Landau-level fan diagrams do not show a notable difference we will use the axial approximation in the following. As a result of the inverted band structure the lowest Landau level of the $H1$ conduction subband and the highest Landau level of the $H2$ valence subband cross at $B\approx14$ T. Such a behavior is specific for type-III QW's and has been examined theoretically and experimentally (see, for example, Ref. 36). The lowest $H1$ Landau level, which corresponds to the quantum number $N=-2$, has pure heavy-hole character, whereas the other Landau levels of the $H1$ subband are mixed states. The highest $H2$ Landau level with $N=0$ contains both heavy and light states.

C. Exchange interaction in magnetic $Hg_{1-y}Mn_yTe$ QW's

In the presence of a magnetic field, the *sp-d* exchange interaction of the *s*- and *p*-band electrons with the $3d^5$ electrons of Mn in $Hg_{1-y}Mn_yTe$ layer influences the band structure of the QW. Such an interaction can be taken into account by adding an appropriate exchange term (H_{ex}) to the Hamil-

tonian [Eq. (6)] in accordance with Refs. 15 and 28, which leads to

$$H + H_{ex} = H - \sum_{\boldsymbol{R}_n} J(\boldsymbol{r} - \boldsymbol{R}_n)\boldsymbol{\sigma}\boldsymbol{S}_n, \tag{17}$$

where $\boldsymbol{\sigma}$ is the spin operator of the band electrons at the position $\boldsymbol{r}$, $\boldsymbol{S}_n$ is the total spin operator of the nth Mn ion at position $\boldsymbol{R}_n$, and $J(\boldsymbol{r}-\boldsymbol{R}_n)$ is the electron-ion exchange integral. Since the electron wave function is extended, the spin operator $\boldsymbol{S}_n$ can be replaced by the thermal average over all states of Mn moments $\langle S_z\rangle$ for a magnetic field in the z direction (mean-field approximation). Moreover, within the virtual crystal approximation, $J(\boldsymbol{r}-\boldsymbol{R}_n)$ can be replaced by $yJ(\boldsymbol{r}-\boldsymbol{R})$, where y is mole fraction of Mn and the summation is now carried out over all cation sites. The exchange term in Eq. (17) then becomes[28]

$$H_{ex} = -\sigma_z\langle S_z\rangle y\sum_{\boldsymbol{R}} J(\boldsymbol{r}-\boldsymbol{R}). \tag{18}$$

The average $\langle S_z\rangle$ of the z component of Mn spin is determined by the empirical expression[37]

$$\langle S_z\rangle = -S_0 B_{5/2}\left(\frac{5g_{Mn}\mu_B B}{2k_B(T+T_0)}\right), \tag{19}$$

where $B_{5/2}(Z)$ is the Brillouin function for a spin of $S=5/2$, $g_{\mathrm{Mn}}=2$ is the g factor of Mn, and the effective spin S_0 and the effective temperature $(T+T_0)$ account for the existence of clusters and antiferromagnetic interaction between Mn ions. The values for S_0 and T_0 are taken from the literature.[3]

The matrix elements of H_{ex} in terms of the Bloch functions [Eqs. (5)] have the form

$$H_{ex} = \begin{pmatrix}
3A\frac{\alpha}{\beta} & 0 & 0 & 0 & 0 & 0 & 0 & 0 \\
0 & -3A\frac{\alpha}{\beta} & 0 & 0 & 0 & 0 & 0 & 0 \\
0 & 0 & 3A & 0 & 0 & 0 & 0 & 0 \\
0 & 0 & 0 & A & 0 & 0 & -2\sqrt{2}A & 0 \\
0 & 0 & 0 & 0 & -A & 0 & 0 & -2\sqrt{2}A \\
0 & 0 & 0 & 0 & 0 & -3A & 0 & 0 \\
0 & 0 & 0 & -2\sqrt{2}A & 0 & 0 & -A & 0 \\
0 & 0 & 0 & 0 & -2\sqrt{2}A & 0 & 0 & A
\end{pmatrix}, \tag{20}$$

with

$$A = -\frac{1}{6}yN_0\beta\langle S_z\rangle. \tag{21}$$

Here, N_0 is the number of unit cells per unit volume; α and β are constants which describe the exchange interaction according to the s-d and p-d exchange integrals, respectively. Experimental values for α and β can be found, for example, in Ref. 26.

The sp-d exchange interaction changes the spin splitting of the conduction and valence bands in a magnetic field. In the parabolic approximation the effective g factor for the Γ_6 states can be described by the following equation [cf. Eqs. (14), (20), and (21)]:

$$g_{eff} = g^* - \frac{yN_0\alpha\langle S_z\rangle}{\mu_B B}, \tag{22}$$

where g^* is the g factor of the band electrons (without exchange term). The effect of the exchange interaction on the Γ_8 states can be expressed by replacing the parameter κ with

$$\kappa_{eff} = \kappa + \frac{yN_0\beta\langle S_z\rangle}{6\mu_B B}. \tag{23}$$

A more detailed model which describes the influence of the Mn ions on the band structure of $A^{\mathrm{II}}\mathrm{Mn}B^{\mathrm{VI}}$ DMS alloys was presented by Hui *et al.*[38] This approach considers the Mn d states and their hybridization with the sp bands explicitly. These authors find that for low Mn concentrations ($y=0.02$) the influence of sp-d hybridization is negligible (cf. Ref. 38). We thus restrict ourselves to the phenomenological mean-field approximation which has already been shown to be in good agreement with experimental data for narrow-gap DMS's.[25]

The influence of the sp-d exchange interaction on the band structure is obvious when we compare the Landau levels in Fig. 2 for the nonmagnetic structure with that in Fig. 3

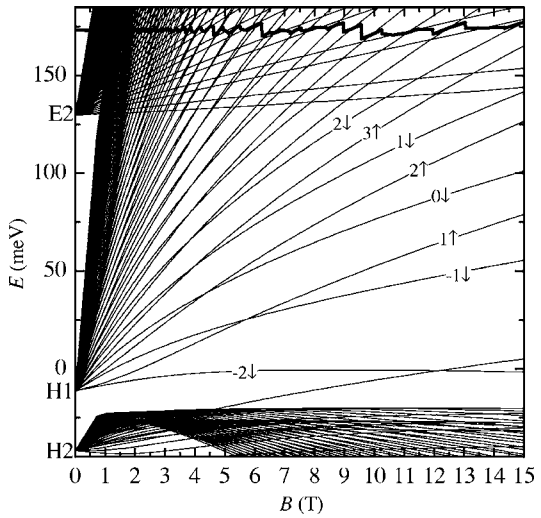

FIG. 3. Landau levels of the $E2$, $H1$, and $H2$ subbands for an n-type $Hg_{0.98}Mn_{0.02}Te/Hg_{0.3}Cd_{0.7}Te(001)$ QW as a function of magnetic field ($d_W=12.2$ nm, $n_{2DEG}=3.47\times10^{12}$ cm^{-2}, $n_{DL}=-0.34n_{2DEG}$, and $T=4.2$ K). The thick line represents the chemical potential. As in Fig. 2, the Landau levels are labeled with quantum numbers N, and the arrows ($\uparrow,\downarrow$) indicate the dominant spin orientation of the state.

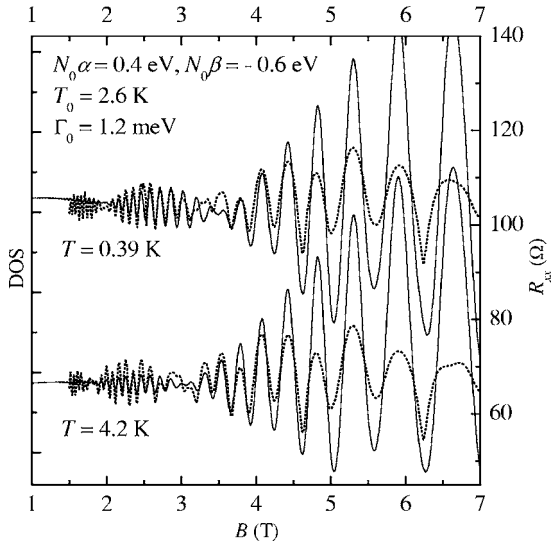

FIG. 4. Density of states of the n-type $Hg_{0.98}Mn_{0.02}Te/Hg_{0.3}Cd_{0.7}Te$ QW at the Fermi level (dotted lines) compared with experimental SdH oscillations (solid lines).

for a magnetic $Hg_{0.98}Mn_{0.02}Te/Hg_{0.3}Cd_{0.7}Te(001)$ QW. The QW width, 2DEG density, and temperature are the same in both cases and identical to those of an actual sample of which the experimental magnetoresistance data were presented in Ref. 3. These experimental results are reproduced here for a comparison with the theory. The subband dispersion for the magnetic QW under consideration is given in Fig. 1(d). The parameters $N_0\alpha=0.4$ eV, $N_0\beta=-0.6$ eV, $S_0=5/2$, and $T_0=2.6$ K are taken from the literature.[3,26] Due to the exchange interaction, the lowest $H1$ Landau level with quantum number $N=-2$ (which contains pure $|\Gamma_8,-3/2\rangle$ Bloch components) is bent upwards for low magnetic fields. In contrast to the nonmagnetic case, pairs of Landau levels from the $H1$ subband cross even at moderate magnetic fields. At high magnetic fields the ordering of the levels is the same as for nonmagnetic structures (Fig. 2). Such behavior was also reported for n-type $Hg_{1-y}Mn_yTe$ mixed crystals.[39] The crossing of the lowest Landau level of the $H1$ subband with the $N=0$ Landau level of the $H2$ subband occurs at lower magnetic fields ($B\approx12$ T) due to the exchange-enhanced shift towards higher energy of the $H2$ level.

In order to compare the calculations with the experimental data, the density of states (DOS) at the Fermi level has to be calculated from the Landau level spectrum (Fig. 3), because experimentally the Landau-level structure becomes visible through the magnetic field dependence of the longitudinal resistance. The Shubnikov–de Haas (SdH) oscillations which are observed in the experiments are directly related to changes of the DOS at the Fermi energy. Assuming a Gaussian broadening of the Landau levels, the DOS is given by[40]

$$\mathrm{DOS}(E)=\frac{1}{2\pi l_c^2}\sum_n\frac{1}{\sqrt{\pi\Gamma^2}}\exp\left(-\frac{(E-E_n)^2}{\Gamma^2}\right), \qquad (24)$$

where the summation runs over all Landau levels. $\Gamma=\Gamma_0\sqrt{B/B_0}$ ($B_0=1$ T) is the Landau-level broadening parameter.[41] In Fig. 4 the calculated DOS is displayed together with the SdH measurement for two different temperatures. The broadening parameter used is $\Gamma_0=1.2$ meV. The main features such as oscillation period, beating nodes, and maxima are in good agreement. The node positions shift to higher magnetic fields with decreasing temperature, which is expected from the Brillouin description of Mn ion magnetization. For a more quantitative comparison the magnetic field dependence of the diffusion constant has to be taken into account.[41]

III. CONCLUSION

A detailed description has been presented of self-consistent band structure calculations within an eight-band $\boldsymbol{k}\cdot\boldsymbol{p}$ model in the envelope function approach with a special emphasis on type-III $HgTe/Hg_{1-x}Cd_xTe$ QW structures. This model is an important tool for the interpretation of both optical[18,23] and transport[9] experiments, where strong spin-orbit subband splitting effects are observed. The model has been adopted to account for *sp-d* exchange effects when magnetic (Mn) ions are introduced into the structures. Self-consistently calculated band structure and DOS are in good agreement with experimental transport results for $Hg_{0.98}Mn_{0.02}Te/Hg_{0.3}Cd_{0.7}Te$ QW's. The calculated band

structure of $Hg_{1-y}Mn_yTe/Hg_{1-x}Cd_xTe$ QW's and the ensuing comparison with experimental data make it possible to understand the mutual influence of the *sp-d* exchange interaction and the two-dimensional confinement effects on the transport properties. Moreover, the effect of the QW parameters (width, doping profile, etc.) on the values of α, β, S_0, and T_0 can now be studied by a direct comparison of experimental data and band structure calculations.

ACKNOWLEDGMENTS

We thank R.R. Gerhardts, J. Sinova, and A.H. MacDonald for fruitful discussions. Financial support from the Deutsche Forschungsgemeinschaft (Grant Nos. SFB410 and GZ:436 WER) is gratefully acknowledged.

APPENDIX A: BOUNDARY CONDITIONS

Since the same basis set u_n is used for the well and the barrier layers in the expansion of Eq. (1) each of the envelope functions $f_n(z)$ is continuous throughout the structure, even at abrupt interfaces.[10] After integrating the effective-mass equation [Eq. (3)] across the interfaces we find the requirement of continuity for $D\boldsymbol{f}$[10,20] where

$$D=\begin{pmatrix} t & 0 & 0 & 0 & 0 & 0 & 0 & 0 \\ 0 & t & 0 & 0 & 0 & 0 & 0 & 0 \\ 0 & 0 & u+v & -\bar{s}_- & 0 & 0 & \frac{1}{\sqrt{2}}\bar{s}_- & 0 \\ -i\sqrt{\frac{2}{3}}P & 0 & -\bar{s}'_+ & u-v & c & 0 & \sqrt{2}v & -\sqrt{\frac{3}{2}}\tilde{s}_- \\ 0 & -i\sqrt{\frac{2}{3}}P & 0 & c^* & u-v & \bar{s}'_- & -\sqrt{\frac{3}{2}}\tilde{s}_+ & -\sqrt{2}v \\ 0 & 0 & 0 & 0 & \bar{s}_+ & u+v & 0 & \frac{1}{\sqrt{2}}\bar{s}_+ \\ i\frac{1}{\sqrt{3}}P & 0 & \frac{1}{\sqrt{2}}\bar{s}'_+ & \sqrt{2}v & -\sqrt{\frac{3}{2}}\tilde{s}'_- & 0 & u & c \\ 0 & -i\frac{1}{\sqrt{3}}P & 0 & -\sqrt{\frac{3}{2}}\tilde{s}'_+ & -\sqrt{2}v & \frac{1}{\sqrt{2}}\bar{s}'_- & c^* & u \end{pmatrix}, \tag{A1}$$

and $\boldsymbol{f}$ is an eight-component envelope function vector. Here,

$$t=-\frac{\hbar^2}{2m_0}(2F+1)\frac{\partial}{\partial z},$$

$$u=\frac{\hbar^2}{2m_0}\gamma_1\frac{\partial}{\partial z},$$

$$v=-\frac{\hbar^2}{m_0}\gamma_2\frac{\partial}{\partial z},$$

$$\bar{s}_\pm=\frac{\hbar^2}{2m_0}i\sqrt{3}(\gamma_3-\kappa)k_\pm,$$

$$\bar{s}'_\pm=\frac{\hbar^2}{2m_0}i\sqrt{3}(\gamma_3+\kappa)k_\pm,$$

$$\tilde{s}_\pm=\frac{\hbar^2}{2m_0}i\sqrt{3}\left(\gamma_3+\frac{\kappa}{3}\right)k_\pm,$$

$$\tilde{s}'_\pm=\frac{\hbar^2}{2m_0}i\sqrt{3}\left(\gamma_3-\frac{\kappa}{3}\right)k_\pm,$$

$$c=\frac{\hbar^2}{m_0}i\kappa k_-, \tag{A2}$$

and the terms involving P are zero if P is constant throughout the structure.

The boundary conditions given above are automatically satisfied through the correct operator ordering in the Hamiltonian [Eq. (6)] and the proper expansion of the envelope functions $f_n(z)$ in terms of the complete set $\{g_i(z)\}$ [Eq. (4)]. The well and the barrier layers of the QW are considered to be a period (with the width d) of a superlattice with the appropriate barrier thickness, which corresponds in practice to an isolated QW. The functions $g_i(z)$ are derived for this two-layer system (well and barrier) from the Legendre polynomials in such a way that they obey conditions of periodicity $[g_i(z)=g_i(z+d)]$ and continuity. The periodicity of the $g_i(z)$ is used to find the matrix elements of the Hamiltonian

[Eq. (6)] in the basis of $\{g_i(z)\}$: $\langle g_j|H_{nn'}|g_i\rangle$. Here, the matrix elements $\langle g_j|\gamma(z)|g_i\rangle$, $\langle g_j|\gamma(z)\frac{\partial}{\partial z}|g_i\rangle$, $\langle g_j|\frac{\partial}{\partial z}\gamma(z)|g_i\rangle$, and $\langle g_j|\frac{\partial}{\partial z}\gamma(z)\frac{\partial}{\partial z}|g_i\rangle$ can be determined exactly by applying the recurrence relations for Legendre polynomials and their derivatives,[42] where $\gamma(z)$ has a constant value for each of the layers of the QW. The matrix elements for the Hartree potential $\langle g_j|V(z)|g_i\rangle$ are then calculated numerically. These calculations lead to a matrix representation of the eigenvalue problem which is solved by matrix diagonalization.

APPENDIX B: CORRECTIONS TO THE MATRIX ELEMENTS OF THE HAMILTONIAN FOR THE [*kkl*] GROWTH DIRECTION

The approach of Los *et al.*[24] can be used to carry out calculations for (*kkl*)-oriented QW's. Since the Γ_6 states as well as the coupling between Γ_6 and Γ_8 (Γ_7) bands are spherically symmetric, only the Bloch basis functions $u_i(\boldsymbol{r})$ $(i=3,\ldots,8)$ [Eqs. (5)] have to be transformed into symmetry-adapted basis functions $u_i(\boldsymbol{r}')$. In addition, the coordinate system is rotated to (x',y',z') such that the z' axis is oriented along the $[kkl]$ growth direction. The corresponding terms are added to the matrix elements of Eqs. (7). The corrections which depend on k and l $(h=l/k)$ are as follows (for simplicity the new coordinates are referred as x,y,z) (Ref. 6):

$$\Delta V = \Delta V_a + \Delta V_c,$$

$$\Delta V_a = -\frac{\hbar^2}{2m_0}\frac{6}{(h^2+2)^2}(2h^2+1)(\mu k_\parallel^2 - 2k_z\mu k_z),$$

$$\Delta V_c = -\frac{\hbar^2}{2m_0}\frac{6}{(h^2+2)^2}(h^2-1)[\mu(k_x^2-k_y^2) - h\sqrt{2}k_x\{\mu,k_z\}], \tag{B1}$$

$$\Delta R = \Delta R_a + \Delta R_c,$$

$$\Delta R_a = \frac{\hbar^2}{2m_0}\frac{\sqrt{3}}{(h^2+2)^2}(2h^2+1)\mu k_-^2,$$

$$\Delta R_c = \frac{\hbar^2}{2m_0}\frac{\sqrt{3}}{(h^2+2)^2}((2h^4+6h^2+1)\mu k_+^2 + 2(h^2-1)(\mu k_\parallel^2 - 2k_z\mu k_z) + h\sqrt{2}[(h^2+5)k_+ - (h^2-1)k_-]\{\mu,k_z\}), \tag{B2}$$

$$\Delta S_\pm = \Delta\bar{S}_\pm = \Delta\tilde{S}_\pm = \Delta S_{a\pm} + \Delta S_{c\pm},$$

$$\Delta S_{a\pm} = \frac{\hbar^2}{2m_0}\frac{4\sqrt{3}}{(h^2+2)^2}(2h^2+1)k_\pm\{\mu,k_z\},$$

$$\Delta S_{c\pm} = \frac{\hbar^2}{2m_0}\frac{\sqrt{6}}{(h^2+2)^2}[2h(h^2-1)(\mu k_\parallel^2 - 2k_z\mu k_z) + h(h^2-1)\mu k_\pm^2 - h(h^2+5)\mu k_\mp^2 + 2\sqrt{2}(h^2-1)k_\mp\{\mu,k_z\}]. \tag{B3}$$

The above terms are separated into axial (index a) and cubic (index c) components. It can be shown that the axial and nonaxial approximations give the same result only for (001)- and (111)-oriented structures at $k_\parallel=0$.

APPENDIX C: INFLUENCE OF STRAIN AND PIEZOELECTRIC EFFECTS

The effects of strain due to the lattice mismatch between HgTe and $Hg_{1-x}Cd_xTe$ can be taken into consideration by applying a formalism introduced by Bir and Pikus.[43] Terms proportional to the strain tensor $\boldsymbol{\epsilon}$ are added to the matrix elements of the Hamiltonian [Eq. (6)]; $H_{nn'}+H_{nn'}^{BP}$. The Bir-Pikus Hamiltonian H^{BP} is derived from Eq. (6) by the following substitution:

$$k_ik_j \rightarrow \epsilon_{ij}. \tag{C1}$$

The strain tensor components (ϵ_{ij}) transform as the product k_ik_j and are determined using the model of De Caro and Tapfer.[44] The band structure parameters have to be replaced by the deformation potentials:

$$\frac{\hbar^2}{2m_0}(2F+1) \rightarrow C,$$

$$\frac{\hbar^2}{m_0}\gamma_1 \rightarrow -2a,$$

$$\frac{\hbar^2}{m_0}\gamma_2 \rightarrow -b,$$

$$\frac{\hbar^2}{m_0}\gamma_3 \rightarrow -\frac{1}{\sqrt{3}}d. \tag{C2}$$

Here, C and a are the hydrostatic and b and d the uniaxial deformation potentials. Due to the strain, the coupling matrix elements between the Γ_6 and the Γ_8, Γ_7 bands have additional terms which are proportional to the Kane momentum matrix element P.[35] These elements are actually quite small and consequently are neglected here. The Bir-Pikus Hamiltonian for (001)-oriented QW's can be written as[6]

$$H^{BP}=\begin{pmatrix} T_\epsilon & 0 & 0 & 0 & 0 & 0 & 0 & 0 \\ 0 & T_\epsilon & 0 & 0 & 0 & 0 & 0 & 0 \\ 0 & 0 & U_\epsilon+V_\epsilon & S_\epsilon & R_\epsilon & 0 & -\frac{1}{\sqrt{2}}S_\epsilon & -\sqrt{2}R_\epsilon \\ 0 & 0 & S_\epsilon^\dagger & U_\epsilon-V_\epsilon & 0 & R_\epsilon & \sqrt{2}V_\epsilon & \sqrt{\frac{3}{2}}S_\epsilon \\ 0 & 0 & R_\epsilon^\dagger & 0 & U_\epsilon-V_\epsilon & -S_\epsilon & \sqrt{\frac{3}{2}}S_\epsilon^\dagger & -\sqrt{2}V_\epsilon \\ 0 & 0 & 0 & R_\epsilon^\dagger & -S_\epsilon^\dagger & U_\epsilon+V_\epsilon & \sqrt{2}R_\epsilon^\dagger & -\frac{1}{\sqrt{2}}S_\epsilon^\dagger \\ 0 & 0 & -\frac{1}{\sqrt{2}}S_\epsilon^\dagger & \sqrt{2}V_\epsilon & \sqrt{\frac{3}{2}}S_\epsilon & \sqrt{2}R_\epsilon & U_\epsilon & 0 \\ 0 & 0 & -\sqrt{2}R_\epsilon^\dagger & \sqrt{\frac{3}{2}}S_\epsilon^\dagger & -\sqrt{2}V_\epsilon & -\frac{1}{\sqrt{2}}S_\epsilon & 0 & U_\epsilon \end{pmatrix}, \tag{C3}$$

where

$$T_\epsilon = C\mathrm{tr}(\epsilon),$$

$$U_\epsilon = a\mathrm{tr}(\epsilon),$$

$$V_\epsilon = \frac{1}{2}b(\epsilon_{xx}+\epsilon_{yy}-2\epsilon_{zz}),$$

$$S_\epsilon = -d(\epsilon_{xz}-i\epsilon_{yz}),$$

$$R_\epsilon = -\frac{\sqrt{3}}{2}b(\epsilon_{xx}-\epsilon_{yy})+id\epsilon_{xy}. \tag{C4}$$

Here $\mathrm{tr}(\epsilon)=\epsilon_{xx}+\epsilon_{yy}+\epsilon_{zz}$ is the trace of the strain tensor.

For (kkl)-oriented structures the Hamiltonian should be presented in the symmetry-adapted set of basis functions as described in Appendix B. The transformed Hamiltonian has the form of Eq. (C3), with appropriate corrections to the matrix elements. These corrections can be derived from Eqs. (B1)–(B3) by the substitutions indicated in Eqs. (C1) and (C2).

If the strain tensor has nonzero off-diagonal components (shear components), internal electric fields are generated in the QW due to the piezoelectric effect. We have calculated the strain-induced polarization and electric fields as described in Ref. 44 and have found that the influence of piezoelectric fields on the band structure of fully strained $HgTe/Hg_{1-x}Cd_xTe$ (112) heterostructures is negligible.[18]

*Electronic address: novik@physik.uni-wuerzburg.de
†Also at School of Physics and Astronomy, University of Nottingham, Nottingham NG7 2RD, UK, and Physics Department, University of Texas at Austin, Austin, TX 78712-0264, USA.

[1] T. Hayashi, M. Tanaka, K. Seto, T. Nishinaga, H. Shimada, and K. Ando, J. Appl. Phys. **83**, 6551 (1998).
[2] A. V. Scherbakov, D. R. Yakovlev, A. V. Akimov, I. A. Merkulov, B. König, W. Ossau, L. W. Molenkamp, T. Wojtowicz, G. Karczewski, G. Cywinski, and J. Kossut, Phys. Rev. B **64**, 155205 (2001).
[3] Y. S. Gui, C. R. Becker, J. Liu, V. Daumer, V. Hock, H. Buhmann, and L. W. Molenkamp, Europhys. Lett. **65**, 393 (2004).
[4] C. Camilleri, F. Teppe, D. Scalbert, Y. G. Semenov, M. Nawrocki, M. Dyakonov, J. Cibert, S. Tatarenko, and T. Wojtowicz, Phys. Rev. B **64**, 085331 (2001).
[5] D. D. Awschalom and N. Samarth, J. Magn. Magn. Mater. **200**, 130 (1999).
[6] A. Pfeuffer-Jeschke, Ph.D. thesis, Physikalisches Institut, Universität Würzburg, Germany, 2000.
[7] G. Bastard, *Wave Mechanics Applied to Semiconductor Heterostructures* (Halsted Press, New York, 1988).
[8] B. Das, S. Datta, and R. Reifenberger, Phys. Rev. B **41**, 8278 (1990).
[9] X. C. Zhang, A. Pfeuffer-Jeschke, K. Ortner, V. Hock, H. Buhmann, C. R. Becker, and G. Landwehr, Phys. Rev. B **63**, 245305 (2001).
[10] M. G. Burt, J. Phys.: Condens. Matter **11**, R53 (1999); **4**, 6651 (1992).
[11] E. O. Kane, in *Physics of III-V-Compounds*, edited by R. K. Willardson and A. C. Beer, Vol. 1 of Semiconductors and Semimetals (Academic Press, New York, London, 1966), p. 75.
[12] E. O. Kane, J. Phys. Chem. Solids **1**, 249 (1957).

[13] J. M. Luttinger, Phys. Rev. **102**, 1030 (1956).
[14] C. R. Pidgeon and R. N. Brown, Phys. Rev. **146**, 575 (1966).
[15] R. Winkler, *Spin Orbit Coupling Effects in Two-Dimensional Electron and Hole Systems* (Springer, Berlin, Heidelberg, 2003).
[16] M. H. Weiler, in *Defects, (HgCd)Se, (HgCd)Te*, edited by R. K. Willardson and A. C. Beer, Vol. 16 of Semiconductors and Semimetals (Academic Press, New York, 1981), p. 119.
[17] J. P. Laurenti, J. Camassel, A. Bouhemadou, B. Toulouse, R. Legros, and A. Lusson, J. Appl. Phys. **67**, 6454 (1990).
[18] C. R. Becker, V. Latussek, A. Pfeuffer-Jeschke, G. Landwehr, and L. W. Molenkamp, Phys. Rev. B **62**, 10353 (2000).
[19] C. K. Shih and W. E. Spicer, Phys. Rev. Lett. **58**, 2594 (1987).
[20] B. A. Foreman, Phys. Rev. B **48**, R4964 (1993).
[21] A. T. Meney, B. Gonul, and E. P. O'Reilly, Phys. Rev. B **50**, 10893 (1994).
[22] B. A. Foreman, Phys. Rev. B **56**, R12748 (1997).
[23] C. R. Becker, V. Latussek, G. Landwehr, and L. W. Molenkamp, Phys. Rev. B **68**, 035202 (2003).
[24] J. Los, A. Fasolino, and A. Catellani, Phys. Rev. B **53**, 4630 (1996).
[25] *Diluted Magnetic Semiconductors*, edited by J. K. Furdyna and J. Kossut, Vol. 25 of Semiconductors and Semimetals (Academic Press, Boston, 1988).
[26] J. Kossut and W. Dobrowolski, in *Narrow Gap II-VI Compounds for Optoelectronic and Electromagnetic Applications*, edited by P. Capper (Chapman & Hall, London, 1997), p. 401.
[27] *Semimagnetic Semiconductors and Diluted Magnetic Semiconductors*, edited by M. Averous and M. Balkanski (Plenum Press, New York, 1991).
[28] J. K. Furdyna, J. Appl. Phys. **64**, R29 (1988).
[29] G. Grabecki, T. Dietl, J. Kossut, and W. Zawadzki, Surf. Sci. **142**, 588 (1984); V. F. Radantsev, A. M. Yafyasov, and V. B. Bogevolnov, Semicond. Sci. Technol. **16**, 320 (2001).
[30] G. Grabecki, T. Dietl, P. Sobkowicz, J. Kossut, and W. Zawadzki, Appl. Phys. Lett. **45**, 1214 (1984); P. Sobkowicz, G. Grabecki, P. Wisniewski, T. Suski, and T. Dietl, in *Proceedings of the 19th International Conference on the Physics of Semiconductors, Warszawa, 1988*, edited by W. Zawadzki (Institute of Physics, Polish Academy of Sciences, Warsaw, 1988), p. 611.
[31] M. von Truchsess, A. Pfeuffer-Jeschke, V. Latussek, C. R. Becker, and E. Batke, J. Cryst. Growth **184/185**, 1190 (1998); M. Fornari, H. H. Chen, L. Fu, R. D. Graft, D. J. Lohrmann, S. Moroni, G. Pastori Parravicini, L. Resca, and M. A. Stroscio, Phys. Rev. B **55**, 16339 (1997).
[32] T. Ando, J. Phys. Soc. Jpn. **51**, 3893 (1982).
[33] Y. S. Gui, C. R. Becker, N. Dai, J. Liu, Z. J. Qiu, E. G. Novik, M. Schäfer, X. Z. Shu, J. H. Chu, H. Buhmann, and L. W. Molenkamp, Phys. Rev. B **70**, 115328 (2004).
[34] J. M. Luttinger and W. Kohn, Phys. Rev. **97**, 869 (1955).
[35] H.-R. Trebin, U. Rössler, and R. Ranvaud, Phys. Rev. B **20**, 686 (1979).
[36] M. Schultz, U. Merkt, A. Sonntag, U. Rössler, R. Winkler, T. Colin, P. Helgesen, T. Skauli, and S. Løvold, Phys. Rev. B **57**, 14772 (1998).
[37] A. Witowski, K. Pastor, and J. K. Furdyna, Phys. Rev. B **26**, 931 (1982).
[38] P. M. Hui, H. Ehrenreich, and K. C. Hass, Phys. Rev. B **40**, 12346 (1989).
[39] M. Jaczyński, J. Kossut, and R. R. Galazka, Phys. Status Solidi B **88**, 73 (1978).
[40] R. R. Gerhardts, Surf. Sci. **58**, 227 (1976).
[41] T. Ando, A. B. Fowler, and F. Stern, Rev. Mod. Phys. **54**, 437 (1982).
[42] Handbook of Mathematical Functions, edited by M. Abramowitz and I. A. Stegun (National Bureau of Standards, Washington, DC, 1964).
[43] G. L. Bir and G. E. Pikus, *Symmetry and Strain-induced Effects in Semiconductors* (Wiley, Chichester, 1974).
[44] L. De Caro and L. Tapfer, Phys. Rev. B **51**, 4374 (1995).